



1 **Comprehensive Quantification of Height Dependence of**  
2 **Entrainment-Mixing between Stratiform Cloud Top and**  
3 **Environment**

4 Sinan Gao<sup>1</sup>, Chunsong Lu<sup>1\*</sup>, Yangang Liu<sup>2</sup>, Seong Soo Yum<sup>3</sup>, Jiashan Zhu<sup>1</sup>, Lei Zhu<sup>1</sup>, Neel Desai<sup>2a</sup>,  
5 Yongfeng Ma<sup>4</sup>

6 <sup>1</sup>Collaborative Innovation Center on Forecast and Evaluation of Meteorological Disasters, Key Laboratory for Aerosol-Cloud-  
7 Precipitation of China Meteorological Administration, Nanjing University of Information Science & Technology, Nanjing,  
8 China

9 <sup>2</sup>Environmental and Climate Sciences Department, Brookhaven National Laboratory, Upton NY, US

10 <sup>3</sup>Department of Atmospheric Sciences, Yonsei University, Seoul, South Korea

11 <sup>4</sup>Department of Mechanics & Aerospace Engineering, Southern University of Science and Technology, Shenzhen, China

12 *Correspondence to:* Chunsong Lu ([luchunsong110@gmail.com](mailto:luchunsong110@gmail.com))

13

---

<sup>a</sup> Now at Department of Meteorology and Climate Science, San Jose State University, San Jose, CA



14 **Abstract.** Different entrainment-mixing processes of turbulence are crucial to processes related to clouds; however, only a few  
15 qualitative studies have been concentrated on the vertical distributions of entrainment-mixing mechanisms with low vertical  
16 resolutions. To quantitatively study vertical profiles of entrainment-mixing mechanisms with a high resolution, the stratiform  
17 clouds observed in the Physics of Stratocumulus Top (POST) project are examined. The unique sawtooth flight pattern allows  
18 for an examination of the vertical distributions of entrainment-mixing mechanisms with a 5 m vertical resolution. Relative  
19 standard deviation of volume mean radius divided by relative standard deviation of liquid water content is introduced to be a  
20 new estimation of microphysical homogeneous mixing degree, to overcome difficulties of determining the adiabatic  
21 microphysical properties required in existing measures. The vertical profile of this new measure indicates that entrainment-  
22 mixing mechanisms become more homogeneous with decreasing altitudes and are consistent with the dynamical measures of  
23 Damkohler number and transition scale number. Further analysis shows that the vertical variation of entrainment-mixing  
24 mechanisms with decreasing altitudes is due to the increases of turbulent dissipation rate in cloud and relative humidity in  
25 droplet-free air, and the decrease of size of droplet-free air. The results offer insights into the theoretical understanding and  
26 parameterizations of vertical variation of entrainment-mixing mechanisms.

27



## 28 **1 Introduction**

29 Clouds are identified to be a significant origin of uncertainties in climate research, because of poor simulations of clouds  
30 (Bony and Dufresne, 2005; Stephens, 2005; Zheng and Rosenfeld, 2015; Zhao and Garrett, 2015; Wang et al., 2019; Cess et  
31 al., 1989; Wang, 2015; Gao et al., 2016; Grabowski, 2006; Morrison, 2015). Entrainment-mixing processes of turbulence have  
32 been considered as significant factors for various processes related to clouds (Su et al., 1998; Lasher - trapp et al., 2005;  
33 Hoffmann and Feingold, 2019; Xu et al., 2020; Hudson et al., 1997; Liu et al., 2002). Therefore, it is vital to figure out the  
34 nature of interaction between clouds and environment and their impacts on cloud droplet properties (Xue and Feingold, 2006).  
35 Entrainment-mixing processes are considered to occur primarily near the stratiform cloud top and entrainment-mixing around  
36 the stratiform cloud sides is negligible (Wood, 2012; Xu and Xue, 2015).

37

38 The question about how entrained air affects cloud microphysics has been debated for a long time. Several conceptual models  
39 have been established to study the different entrainment-mixing processes, e.g., entity-type entrainment-mixing (Telford, 1996;  
40 Telford and Chai, 1980), vertical circulation entrainment-mixing (Yeom et al., 2017; Yum et al., 2015; Wang et al., 2009) and  
41 homogeneous (HM)/inhomogeneous (IM) entrainment-mixing (Baker et al., 1980; Baker et al., 1984). The last one is the most  
42 used and studied. During the HM mixing, the time scale for droplets to evaporate completely is larger than the time scale for  
43 mixing between entrained air and cloudy air. All droplets are exposed to the same unsaturated state and evaporate concurrently.  
44 In this scenario, all droplets' sizes decrease simultaneously, and number concentration also decreases due to the dilution effect  
45 of entrained air. While in the IM mixing, mixing time scale is larger than evaporation time scale. Some droplets adjacent to  
46 entrained air would evaporate completely to saturate the air, while the other droplets are not affected by the entrainment. In  
47 this scenario, number concentration decreases but droplet size remains unchanged. Some observational studies support the  
48 extreme IM concept (Burnet and Brenguier, 2007; Lu et al., 2011; Freud et al., 2011; Pawlowska et al., 2000; Haman et al.,  
49 2007; Freud et al., 2008); while some others indicate that the HM mixing dominates (Gerber et al., 2008; Lu et al., 2013c;  
50 Burnet and Brenguier, 2007; Jensen et al., 1985), and still some others find intermediate features fall in between the HM and  
51 IM mixing (Lehmann et al., 2009; Lu et al., 2014a; Kumar et al., 2018).

52

53 The vertical variation of entrainment-mixing mechanisms is less studied. For cumulus, Small et al. (2013) and Jarecka et al.  
54 (2013) found that a trend existed of entrainment-mixing to be more HM in cloud top, resulted from increasing of cloud droplet  
55 radius and turbulence with increasing altitudes. In stratiform clouds, Yum et al. (2015) and Wang et al. (2009) observed positive  
56 correlation at middle of cloud and no correlation at cloud top between droplet size and liquid water content. Yum et al. (2015)  
57 suggested that entrainment mixing at cloud top region was indeed IM, while during the descent of vertical circulation, the  
58 cloud droplets in more diluted parcels would evaporate faster, and observe the generally HM feature at a relatively long depth



59 from cloud top.

60

61 The above few studies are largely qualitative and based on horizontal flight legs with coarse vertical resolutions. Furthermore,  
62 these studies often need to determine adiabatic cloud microphysical properties from observational data, which are full of known  
63 and unknown uncertainties (e.g., (Jensen et al., 1985; Yum et al., 2015; Lu et al., 2014b; Yeom et al., 2017).

64

65 This study aims to overcome these limitations by examining the data from the field campaign of Physics of Stratocumulus Top  
66 (POST) (Hill et al., 2010; Malinowski et al., 2010; Gerber et al., 2010) for the high-resolution vertical variation of entrainment-  
67 mixing processes. Four measures of microphysical homogeneous mixing degrees (HMDs) that require the determination of  
68 adiabatic cloud properties (Lu et al., 2014b; Lu et al., 2013b; Lu et al., 2014a) are examined and inconsistencies are discussed.  
69 A new microphysical measure is proposed to quantify the entrainment-mixing mechanisms to overcome the drawbacks of the  
70 existing methods that require cloud adiabatic properties. Physical reasons for the vertical variation of entrainment-mixing  
71 mechanisms are analyzed using a comprehensive microphysical-dynamical approach.

72

73 The rest of this study is presented as follows. The POST dataset and the existing methods for calculating microphysical and  
74 dynamical measures of HMD are presented in Section 2. Section 3 first shows the analysis of entrainment-mixing mechanisms  
75 using the existing microphysical measures and dynamical measures. A new microphysical measure is then introduced to  
76 represent entrainment-mixing mechanisms after discussing the potential uncertainties in choosing and determining the  
77 adiabatic properties needed for the existing microphysical measures. The key factors affecting vertical variation of  
78 entrainment-mixing are examined as well. Section 4 is the concluding remarks.

## 79 **2 Dataset and Methods**

### 80 **2.1 Dataset**

81 POST was designed to further the understanding of the physical processes around stratiform cloud top zone (Carman et al.,  
82 2012; Gerber et al., 2010; Hill et al., 2010; Malinowski et al., 2010; Ma et al., 2017; Jen-La Plante et al., 2016; Ma et al., 2018;  
83 Kumala et al., 2013). During POST campaign, thermodynamic, dynamical, and microphysical properties were measured on  
84 board in July and August of 2008 with a total of 17 research flights. Flights were implemented in the vicinity of the coast of  
85 Santa Cruz/Monterey, California, US, within 36° to 37°N and 123° to 124°W (Gerber et al., 2010; Hill et al., 2010; Malinowski  
86 et al., 2010).

87

88 Cloud droplet distributions were from the measurement by the Cloud Aerosol Spectrometer (CAS) probe, and the measured



89 frequency is 10 Hz. The microphysical properties, number concentration ( $n_c$ ), liquid water content ( $LWC_c$ ) and volume mean  
90 radius ( $r_{vc}$ ) are calculated from the cloud droplet distributions using the radius range of 1 - 25  $\mu\text{m}$ . The Modified Ultrafast  
91 Thermometer (UFT-M) was the temperature probe. Only the flights with good quality temperature data (no reports of “noise”,  
92 “spike” or “holes in the data” in the data description file) are used. Although the time resolution of temperature data was as  
93 high as 1000 Hz (Kumala et al., 2013), 10 Hz data are used here. Humidity was measured by the EDGETECH EG&G Chilled  
94 Mirror at 10 Hz. For turbulence measurements, the five-hole gust detector provided by University of California, Irvine (UCI)  
95 was used to collect high resolution wind velocities at 40 Hz. We use  $10\text{ cm}^{-3}$  of  $n_c$  and  $0.001\text{ g m}^{-3}$  of  $LWC_c$  to be the standard  
96 of threshold values to select cloudy samples (Lu et al., 2014b; Deng et al., 2009; Zhang et al., 2011). We define the cloud base  
97 as the lowest altitudes where the samples satisfy the previously mentioned cloud criteria. We focus only on the non-drizzling  
98 clouds, and the threshold value of drizzle water content in cloud using Cloud Imaging Probe (CIP) measurements (radius larger  
99 than 25  $\mu\text{m}$ ) is  $0.005\text{ g m}^{-3}$  (Lu et al., 2011). A total of 4 flights in POST (July 16, August 02, 06, 08, 2008) satisfying the above  
100 criteria is selected to examine the vertical variation of entrainment-mixing mechanisms.

## 101 2.2 Sawtooth Pattern Flights

102 Unlike most aircraft campaigns, the POST flights were designed as sawtooth legs to examine detailly the vertical structures of  
103 the stratiform cloud top zone (Figure 1 (a)) (Carman et al., 2012; Gerber et al., 2013; Jen-La Plante et al., 2016). About 60  
104 sawtooth legs are contained in each flight (Gerber et al., 2013; Carman et al., 2012). In this way, high-resolution vertical  
105 profiles near cloud top can be obtained, which are not available from the conventional sampling along horizontal legs. Because  
106 the cloud top altitudes vary spatially, we calculate the average cloud top altitude measured by each sawtooth profile and only  
107 the sawtooth legs with cloud tops 30 m above/below the average cloud top are selected. The procedure of altitude stratification  
108 is illustrated in Figure 1 (b). We take 5 m as the vertical interval of all sawtooth patterns. All the analyses below are based on  
109 the cloud properties averaged over the 5 m vertical intervals and each vertical interval consists of thousands of data. Only the  
110 height intervals over which the average droplet-free air sizes (i.e., non-cloudy sample sizes between cloudy samples) are larger  
111 than zero are analyzed, which is detailed later in Figure 10. The results are similar when the vertical resolution of all sawtooth  
112 patterns is set as 3 m and 7 m, respectively (not shown).

## 113 2.3 Methods

### 114 2.3.1 Existing Microphysical Measures of Homogeneous Mixing Degree

115 Based on the diagram of microphysical mixing, four HMDs have been defined to contain all kinds of entrainment mixing  
116 mechanisms. The first three measures are based on the diagram of  $r_{vc}^3/r_{va}^3$  versus  $n_c/n_a$  (Lu et al., 2014a; Lu et al., 2013b), as



117 shown in Figure 2 (a) and (b). Figure 2 (a) declares the various status during a whole process of entrainment-mixing for  
 118 defining the first measure ( $\psi_1$ ). The adiabatic cloud is represented by Point A with the number concentration ( $n_a$ ) and volume  
 119 mean radius ( $r_{va}$ ) of adiabatic state. After environmental air is entrained into cloud, the state of cloud approaches Point B,  
 120 where number concentration is  $n_h$  and volume mean radius is  $r_{vh}$ . Then mixing and evaporation processes occur and cloud state  
 121 approaches Point C, where number concentration after evaporation is  $n_c$  and volume mean radius after evaporation is  $r_{vc}$ . The  
 122 included angle between the line connecting Point B to Point E and the extreme IM mixing line is  $\pi/2$ , and the included angle  
 123 between the line connecting Point B to Point C and the extreme IM mixing line is  $\beta$ . Then  $\psi_1$  is defined as:

$$124 \quad \psi_1 = \frac{\beta}{\pi/2}, \quad (1a)$$

125 where  $\beta$  is

$$126 \quad \beta = \arctan\left(\frac{r_{vc}^3/r_{va}^3 - 1}{n_c/n_a - n_h/n_a}\right); \quad (1b)$$

127  $n_h = n_a \times \chi$  and  $\chi$  represents the adiabatic cloud fraction after mixing derived from energy conservation and total water  
 128 conservation in the isobaric mixing (Lehmann et al., 2009; Gerber et al., 2008; Lu et al., 2012). The second HMD ( $\psi_2$ ) is  
 129 defined in view of Figure 1 (b):

$$130 \quad \psi_2 = \frac{1}{2} \left( \frac{n_c - n_i}{n_h - n_i} + \frac{r_{vc}^3 - r_{va}^3}{r_{vh}^3 - r_{va}^3} \right), \quad (2)$$

$$131 \quad \text{where } n_i = \frac{r_{vc}^3}{r_{va}^3} n_c. \quad (3)$$

$$132 \quad r_{vh}^3 = \frac{n_c}{n_h} r_{vc}^3 \quad \text{and} \quad (4)$$

133 Here  $n_i$  is the number concentration after extreme IM mixing and  $r_{vh}$  is the volume mean radius after HM mixing. The third  
 134 measure of HMD ( $\psi_3$ ) is given by

$$135 \quad \psi_3 = \frac{\ln n_c - \ln n_i}{\ln n_h - \ln n_i} = \frac{\ln r_{vc}^3 - \ln r_{va}^3}{\ln r_{vh}^3 - \ln r_{va}^3}. \quad (5)$$

136 The fourth measure ( $\psi_4$ ) is defined using mixing diagram of  $r_{vc}^3/r_{va}^3$  versus  $LWC_c/LWC_a$  (Lu et al., 2014b), as shown in Figure  
 137 2 (c),

$$138 \quad \psi_4 = \frac{1 - r_{vc}^3/r_{va}^3}{1 - LWC_c/(\chi LWC_a)}. \quad (6)$$

139

140 The meanings of the Points A - E are the same as those in Figures 2 (a) and 2 (b). Four kinds of HMDs are expected to range  
 141 from 0 to 1, the higher probability of HM mixing corresponds to the larger HMD value.



### 142 2.3.2 Dynamical Measures of Homogeneous Mixing Degree

143 The dynamical aspect, i.e., the mixing process between cloud and environment air vs. the evaporation process of cloud droplets,  
144 is important to distinguish different entrainment-mixing mechanisms (Baker et al., 1980; Baker and Latham, 1979). The mixing  
145 time scale divided by evaporation time scale is defined as Damkohler number ( $Da$ ), which is usually used to quantify mixing  
146 process is faster or evaporation process is faster and thus to discern the entrainment-mixing mechanisms (Siebert et al., 2006;  
147 Burnet and Brenguier, 2007; Andrejczuk et al., 2009),

$$148 \quad Da = \frac{\tau_{\text{mix}}}{\tau_r}, \quad (7)$$

149 where  $\tau_{\text{mix}}$  and  $\tau_r$  are turbulent mixing time and microphysical response time of droplets, respectively (Lehmann et al., 2009).  
150 A more IM mixing corresponds to a larger  $Da$ . Three kinds of microphysical time scales, phase relaxation time ( $\tau_{\text{phase}}$ ) (Kumar  
151 et al., 2013; Kumar et al., 2012), evaporation time ( $\tau_{\text{evap}}$ ) (Andrejczuk et al., 2009; Baker et al., 1980; Burnet and Brenguier,  
152 2007), and reaction time ( $\tau_{\text{react}}$ ) (Lehmann et al., 2009; Lu et al., 2011; Lu et al., 2013c; Lu et al., 2014b), have been used to  
153 represent  $\tau_r$ . Lu et al. (2018) found that the most appropriate time scale was  $\tau_{\text{evap}}$  if we focus on the changes of number  
154 concentration and radius of droplets. The mixing time scale is defined as follows:

$$155 \quad \tau_{\text{mix}} \sim (L^3 / \varepsilon)^{1/3}, \quad (8)$$

156 where  $\varepsilon$  is the turbulent dissipation rate calculated from the three dimensional wind velocities (Meischner et al., 2001) (see  
157 Appendix A for details), and  $L$  is the size of droplet-free air calculated with

$$158 \quad L = F \times TAS / f, \quad (9)$$

159 where droplet-free sample size divided by the sum of cloud and droplet-free sample size is considered as fraction of droplet-  
160 free  $F$  in each vertical interval (e.g., if there are 90 cloud samples and 10 non-cloudy samples,  $F = 10/(10+90) = 10\%$ );  $TAS$   
161 and  $f$  are the aircraft true air speed ( $\sim 55 \text{ m s}^{-1}$ ) and sampling frequency (10 Hz), respectively. The size of droplet-free air is  
162 used as a proxy for the entrained air parcels' size. In equation (7), the time scale for a droplet of radius  $r_{\text{va}}$  to completely  
163 evaporate (evaporate time) is given by:

$$164 \quad \tau_{\text{evap}} = -\frac{r_{\text{va}}^2}{2AS_0}, \quad (10)$$

165 where  $S_0$  is the supersaturation of the droplet-free air at the corresponding altitude (Yau and Rogers, 1996);  $A$  is affected by  
166 air temperature and pressure (see Appendix B for details).

167

168 Another dynamical measure given by the ratio of  $L^*$  to  $\eta$  is transition scale number ( $N_L$ ) (Lu et al. (2011)):

$$169 \quad N_L = \frac{L^*}{\eta}, \quad (11)$$



170 where transition length ( $L^*$ ) is considered as the corresponding  $L$  value when  $Da = 1$  (Lehmann et al., 2009) and is given as  
171 follows:

$$172 \quad L^* = \varepsilon^{1/2} \tau_r^{3/2}. \quad (12)$$

173 In equation (11),  $\eta$  is the Kolmogorov length scale (Wyngaard, 2010), which is given by:

$$174 \quad \eta = \left(\frac{v^3}{\varepsilon}\right)^{1/4}, \quad (13)$$

175 where  $v$  is the kinematic viscosity (Wyngaard, 2010). A higher probability of HM mixing corresponds to a larger value of  $N_L$ .

## 176 **3 Results**

### 177 **3.1 Entrainment-Mixing Mechanisms from the Microphysical and Dynamical Perspectives**

178 It has been known that it can be uncertain and even problematic to determine the representative adiabatic values from the  
179 observational data needed in calculation of the above-mentioned microphysical measures (Yeom et al., 2017; Jensen et al.,  
180 1985; Yum et al., 2015). For example, because vertical velocity and concentration of cloud condensation nuclei can change  
181 spatially in clouds,  $n_a$  and  $r_{va}$  change accordingly. Entrainment-mixing in clouds adds difficulties to determine accurate values  
182 of  $r_{va}$ ,  $n_a$  and  $LWC_a$ . Improper estimation of adiabatic values may violate the theoretical expectation:  $n_a \geq n_1 \geq n_c \geq n_i$  and  $r_{va} \geq$   
183  $r_v$ , and then cause unrealistic HMDs. Different adiabatic variables have been used in previous studies. For example, the  
184 maximum volume mean radius and number concentration are used as proxy values for  $r_{va}$  and  $n_a$  for each horizontal penetration,  
185 respectively (Yeom et al., 2017; Yum et al., 2015);  $LWC_a$  is calculated from the adiabatic growth from cloud base, and the  
186 maximum number concentration of whole flight penetration is considered as  $n_a$  (Burnet and Brenguier, 2007; Lehmann et al.,  
187 2009);  $n_a$  is the mean value of top 2% of  $n_c$  for each flight and  $r_{va}$  is calculated using adiabatic water vapor mixing ratio,  
188 adiabatic total water mixing ratio and  $n_a$  for a horizontal penetration (Small et al., 2013).

189

190 To examine the influence of using different adiabatic properties, we compare  $\psi_i$  ( $i = 1, 4$ ) calculated with different adiabatic  
191 variables (Table 1) at each level near the stratiform cloud tops for the data collected during the four flights. Only the results  
192 for the first microphysical measure are shown in Figure 3; the other results are shown in the Supporting Information. In Figure  
193 3,  $LWC_a$  is based on the adiabatic growth from cloud base, the maximum number concentration at each level is assumed as  $n_a$ ,  
194 and  $r_{va}$  is calculated from  $LWC_a$  and  $n_a$ . In Figure S1,  $LWC_a$  is based on the adiabatic growth from cloud base, the maximum  
195 volume mean radius at each level is assumed as  $r_{va}$ , and  $n_a$  is calculated from  $LWC_a$  and  $r_{va}$ . In Figure S2, the maximum liquid  
196 water content at each level is assumed as  $LWC_a$ , the maximum number concentration at each level is assumed as  $n_a$ , and  $r_{va}$  is  
197 calculated from  $LWC_a$  and  $n_a$ . In Figure S3, the maximum liquid water content at each level is assumed as  $LWC_a$ , the maximum



198 volume mean radius at each level is assumed as  $r_{va}$ , and  $n_a$  is calculated from  $LWC_a$  and  $r_{va}$ . In Figure S4, the maximum number  
199 concentration at each level is assumed as  $n_a$ , the maximum volume mean radius at each level is assumed as  $r_{va}$ , and  $LWC_a$  is  
200 calculated from  $n_a$  and  $r_{va}$ . According to the definitions,  $\psi_i$  ( $i = 1, 4$ ) are expected to range from 0 to 1. However, some values  
201 of  $\psi_i$  ( $i = 1, 4$ ) are larger than 1 or smaller than 0 in Figure 3 and Figures S1 – S4, which could be caused by uncertainties in  
202  $r_{va}$ ,  $LWC_a$ ,  $n_a$ , and cloud base (Lu et al., 2014b; Lu et al., 2014a; Lu et al., 2013b). Furthermore, these figures suggest different  
203 vertical distributions of HMDs for the same flight, suggesting that high sensitivity of the conventional HMDs to the methods  
204 for determining the adiabatic values could pose a serious problem as to which figure represents the reality of entrainment-  
205 mixing mechanisms.

206

207 Since the above analysis from the microphysical perspective does not tell a consistent story about the vertical variation of  
208 HMD,  $Da$  and  $N_L$  are examined from the dynamical perspective. Figures 4 (a), (c), (e) and (g) show the height dependence of  
209  $Da$  during each of the four flights. It is obvious that  $Da$  decreases with decreasing altitudes. Figures 4 (b), (d), (f) and (h) show  
210 a significant increasing trend of  $N_L$  with decreasing altitudes. The method for setting the adiabatic values in Figure 4 is the  
211 same as that in Figure 3, i.e.,  $LWC_a$  is based on the adiabatic growth from cloud base, the maximum number concentration at  
212 each level is assumed as  $n_a$ , and  $r_{va}$  is calculated from  $LWC_a$  and  $n_a$ . Unlike the microphysical measures, vertical variation of  
213  $Da$  or  $N_L$  are similar when different methods for determining adiabatic values are used (Figures S5 – S8). It is expected that a  
214 smaller  $Da$  (larger  $N_L$ ) represents a larger HMD. The results of  $Da$  and  $N_L$  both suggest more IM mixing closer to cloud top.  
215 It is noteworthy that this result is robust, not affected by the methods for obtaining the adiabatic values, and thus should reflect  
216 the real height dependence of entrainment-mixing mechanisms.

217

218 The different vertical distributions of HMDs and the inconsistency between microphysical HMDs and dynamical measures are  
219 mainly due to the improper estimations of adiabatic values. For example, during the flight of 16 July in Figure 3, the HMDs  
220 decrease with the decreasing altitudes, and most of the HMDs are negative. The negative values do not meet the theoretical  
221 expectations and these trends are completely inconsistent with those of dynamical measures. The vertical variations of some  
222 important properties of this case are shown in Figure 5. The negative values of HMDs are due to unexpected result of  $r_{va} \leq r_{vc}$ .  
223 Under these circumstances, the difference between  $r_{vc}$  and  $r_{va}$  becomes larger with the decreasing altitudes, corresponding to  
224 the decreasing trends of HMDs with the decreasing altitudes. Besides the first method, the other four methods mentioned above  
225 also have their own unreasonable points. For example,  $r_{va} \leq r_{vc}$  exists under the methods 1, 3 and 4;  $n_a \leq n_c$  exists under the  
226 methods 2 and 4;  $r_{va}$  does not always increase with the increasing altitudes under the methods 2, 4 and 5 (See figures S9 to  
227 S13 for details). Overall, the inconsistency among the microphysical HMDs estimated with different methods to determine the  
228 adiabatic variables calls for a new microphysical measure of entrainment-mixing mechanisms.



### 229 3.2 New Microphysical Measure

230 As discussed in Section 3.1, the existing microphysical measures of HMDs depend on the different adiabatic values to a great  
231 extent. In order to avoid this kind of uncertainty, a new dimensionless HMD ( $\psi_5$ ) is introduced to quantify the different  
232 entrainment-mixing mechanisms:

$$233 \psi_5 = \text{dis}(r_{\text{vc}}^3) / \text{dis}(\text{LWC}_c), \quad (14)$$

234 where  $\text{dis}$  represents the relative standard deviation expressed by the ratio of standard deviation to the average value over each  
235 level. During entrainment-mixing and evaporation processes,  $\text{LWC}_c$  always decreases but  $r_{\text{vc}}$  decreases in the HM mixing and  
236 remains constant in the extreme IM mixing. Therefore, the extreme IM mixing corresponds to  $\psi_5 = 0$ , and the larger the value  
237 of  $\psi_5$  is, the more HM the entrainment mixing is. To make sure that  $\psi_5$  is applied properly, the correlation between  $r_{\text{vc}}^3$  and  
238  $\text{LWC}_c$  must be positive. If the correlation is negative, IM mixing with subsequent ascent is likely to occur (Lu et al., 2013a;  
239 Lehmann et al., 2009; Wang et al., 2009; Siebert et al., 2006; Lasher - trapp et al., 2005). It is worth mentioning that  $\psi_5$  does  
240 not require using adiabatic values, and thus can overcome the deficiencies of  $\psi_i$  ( $i = 1, 4$ ) associated with choosing different  
241 adiabatic cloud properties.

242

243 The vertical variation of  $\psi_5$  for the 4 flights are shown in Figure 6. The small value of  $\psi_5$  near the cloud tops shows that  
244 entrainment-mixing approaches extreme IM, consistent with conclusions in several previous studies based on the POST data  
245 (Gerber et al., 2013; Gerber et al., 2016; Malinowski et al., 2013). The increase of  $\psi_5$  with decreasing altitudes indicates that  
246 the trends towards more HM with the decreasing altitudes, consistent with the results of  $Da$  and  $N_L$  (Figure 4 and Figures S5  
247 – S8). We also check the relationship between  $r_{\text{vc}}^3$  and  $\text{LWC}_c$  and the two quantities are positively correlated (not shown).

248

249 The relationships between  $\psi_5$  versus  $Da$  and  $N_L$  of the 4 flights are shown in Figure 7 and are well fitted by the equations used  
250 in Luo et al. (2020)

$$251 \psi_5 = a_1 \exp(b_1 Da^{c_1}), \quad (15)$$

$$252 \psi_5 = a_2 \exp(b_2 N_L^{c_2}), \quad (16)$$

253 where the parameters  $a_1$  and  $a_2$  are positive;  $b_1$  and  $b_2$  are negative;  $c_1$  is positive and  $c_2$  is negative. The negative correlation  
254 of  $\psi_5$  vs  $Da$  and positive correlation of  $\psi_5$  vs  $N_L$  are evident and in keeping with theoretical arguments, suggesting that a smaller  
255  $Da$  or a larger  $N_L$  corresponds to a higher  $\psi_5$ . Such relationships further confirm the utility and applicability of  $\psi_5$  in studying  
256 entrainment-mixing mechanisms. The correlation coefficients of the linear regression of for  $\psi_5$  vs  $Da$  and  $\psi_5$  vs  $N_L$  are about  
257 0.66 and 0.60, respectively, suggesting that  $Da$  and  $N_L$  are basically equivalent for understanding the entrainment-mixing  
258 parameterization.



259

260 The equivalence of  $Da$  and  $N_L$  is further supported by the tight negative correlation between  $Da$  and  $N_L$  (Figure 8). Similar  
261 results have been reported in Gao et al. (2018) using numerical simulations, and Desai et al. (2021) based on holographic  
262 measurements. However, the underlying reasons are different. Figure 9 shows that  $L$  and  $L^*$  are negatively correlated, opposite  
263 to the positive correlation between  $L^*$  and the Taylor microscale in Gao et al. (2018); Taylor microscale is used as  $L$  in the  
264 calculation of  $\tau_{\text{mix}}$  in equation (8) in Gao et al. (2018). It is easy to derive from equations (7), (8), (10) and (11) that  $Da : N_L =$   
265  $L : L^*$ , others being equal:

$$266 \frac{Da}{N_L} = \frac{-2AS_0\eta}{\varepsilon^{1/3}r_{\text{va}}^2} \cdot \frac{L}{L^*} \quad (17)$$

267 Therefore, as long as  $L$  and  $L^*$  are nearly linearly correlated,  $Da$  and  $N_L$  are equivalent. When extreme IM mixing dominates  
268 near cloud top,  $\varepsilon$  is small (Figure 10), which mainly determines small  $L^*$ ;  $L$  is large near cloud top (Figure 10). Therefore,  $L$   
269 and  $L^*$  are negatively correlated. The vertical distributions of affecting factors on entrainment-mixing are detailed in the next  
270 sub-section.

271

### 272 3.3 Further analysis of Affecting Factors

273 According to the analyses in Sections 3.1 and 3.2, the dynamical and microphysical measures both indicate that entrainment-  
274 mixing mechanisms change from IM to HM with decreasing altitudes. Here we provide the physical explanation for such  
275 behavior under the framework of HM/IM entrainment-mixing mechanisms, by analyzing the vertical variations of all the  
276 variables defining  $Da$  and  $N_L$ , i.e.,  $\varepsilon$ , relative humidity (RH) and  $L$ .

277

278 First, Figures 10 (a), (d), (g) and (j) show that  $\varepsilon$  increases with decreasing altitudes, which is opposite to that for cumulus  
279 clouds (Small et al. (2013) and Jarecka et al. (2013)). According to definition of  $Da$  (equation (7)) and  $N_L$  (equation (11)), the  
280 increase of  $\varepsilon$  leads to the decrease of  $Da$  and increase of  $N_L$ , others being equal. Therefore,  $\varepsilon$  is an important factor to cause  $Da$   
281 to decrease and  $N_L$  to increase with the decreasing altitudes (Figure 4 and Figures S5 – S8).

282

283 Second, the vertical variation of entrainment-mixing can also be attributed to that of entrained air sizes. Figures 10 (b), (e), (h)  
284 and (k) show that  $L$  decreases significantly with decreasing altitudes, which leads to a decrease of  $Da$  with decreasing altitudes  
285 since  $Da$  is proportional to  $\tau_{\text{mix}}$ , and thus  $L$ . The importance of  $L$  has rarely been studied in previous literatures for height  
286 dependence of entrainment-mixing. The decrease of  $L$  with decreasing altitudes agrees generally with the cascade of  
287 breakdown of dry air parcels entrained at the cloud top.

288



289 Third, vertical variation of entrained air RH plays a significant part in determining the entrainment-mixing mechanisms. In  
290 former literatures (Yeom et al., 2017; Lu et al., 2018), RH is commonly assumed to be constant across multiple different  
291 altitudes when calculating  $\tau_{\text{evap}}$  using  $S_0 = \text{RH} - 1$ . In fact, RH should not be a constant. We determine RH as the mean RH of  
292 droplet-free air in each level. Figures 10 (c), (f), (i) and (l) show that RH increases with decreasing altitudes due to droplet  
293 evaporation. According to the definition of  $Da$ ,  $Da$  decreases with the increase of  $\tau_{\text{evap}}$ , and thus decreases with the increase of  
294 RH (equation (7) and (10)). Equations (10), (11) and (12) show that  $N_L$  increases with increasing RH. Both  $Da$  and  $N_L$  indicate  
295 more HM mixing at a lower altitude. These results suggest that the increases of  $\varepsilon$  and RH and the decrease of  $L$  with decreasing  
296 altitudes are in keeping with the variation of entrainment-mixing processes, together playing the primary role in determining  
297 the vertical distribution of HMD observed.

298

299 It is noted that,  $r_{\text{va}}$  also affects  $Da$  and  $N_L$  through its effect on  $\tau_{\text{evap}}$ . However,  $r_{\text{va}}$  depends on how adiabatic values are estimated  
300 in Section 3.1 (Figure S9 – S14 in the Supporting Information). Therefore, the vertical variation of  $r_{\text{va}}$  is not analyzed here. No  
301 matter which method is used to determine the adiabatic values, the trends of vertical variation of  $Da$  and  $N_L$  do not change  
302 (Section 3.1). The vertical variation of  $Da$  and  $N_L$  indicates the dominance of the combined effects of  $\varepsilon$ , RH and  $L$  in  
303 determining the vertical variation of entrainment-mixing processes from IM towards HM with decreasing altitudes.

304

305 These results are in keeping with the results drawn in Wang et al. (2009) and Yum et al. (2015) in the sense that a trait of IM  
306 mixing is prevalent near cloud top but at mid-levels of clouds a trait of HM mixing becomes dominant, according to the  
307 analysis of cloud microphysical relationships at different altitudes of marine stratiform clouds. However, there are big  
308 differences in the spatial scale of analysis between our and their studies. We focus on near cloud top regions from cloud top to  
309 where droplet-free air patches can still be found, mostly less than 100 m from cloud top (Figure 3). On the other hand, Yum et  
310 al. (2015) and Wang et al. (2009) examined mid-levels of stratiform clouds where there remained no droplet-free air patches  
311 as well as near cloud top regions. They suggested that the vertical variation of cloud microphysical properties relationships  
312 could be caused by vertical circulation of diluted parcels affected by entrainment; the actual mixing near cloud top might have  
313 been IM as  $Da$  and  $N_L$  at this level suggested; as these parcels moved down, the droplets evaporated fast, resulting in cloud  
314 microphysical relationships that would be explained as a trait of HM mixing.

#### 315 4 Concluding Remarks

316 The observational data of marine stratiform clouds measured from aircraft during the campaign of Physics of Stratocumulus  
317 Top (POST) are used to examine the height dependence of entrainment-mixing mechanisms. The sawtooth penetrations are  
318 analyzed to acquire fine information on the vertical structure of entrainment-mixing near stratiform cloud tops, from the



319 microphysical and dynamical perspectives. To ensure high vertical resolution, we take 5 m as one altitude distance bin of all  
320 sawtooth patterns for the four flights selected in this study.

321

322 From the microphysical perspective, the traditional homogeneous mixing degrees vary distinctly with the decreasing altitudes  
323 due to different methods for obtaining adiabatic values. In order to overcome this difficulty, a new homogeneous mixing degree  
324 describing the distributions of scatters in the mixing diagram is introduced to quantify different entrainment-mixing  
325 mechanisms. The new homogeneous mixing degree is introduced by relative standard deviation of cubic volume mean radius  
326 divided by relative standard deviation of liquid water content. If the new homogeneous mixing degree is larger, the mixing is  
327 more likely to be homogeneous. The new measure increases with the decreasing altitudes, i.e., more homogeneous with  
328 decreasing altitudes. This new measure is not affected by the methods for obtaining adiabatic values and shed new light on the  
329 study of entrainment-mixing mechanisms.

330

331 From the dynamical perspective, Damkohler number decreases and transition scale number increases with decreasing altitudes.  
332 The relationships between the new homogeneous mixing degree vs. Damkohler number and transition scale number are  
333 negative and positive, respectively, consistent with theoretical expectation. Therefore, both microphysical and dynamical  
334 analyses indicate the trends from inhomogeneous mixing to homogeneous mixing when altitude decreases.

335

336 The factors underlying the vertical variation of entrainment-mixing mechanisms are examined, including vertical distributions  
337 of dissipation rate, size of droplet-free air and relative humidity in droplet-free air. Dissipation rate increases and droplet-free  
338 air size decreases with the decreasing altitudes. Therefore, mixing is faster at the lower altitude and homogeneous mixing is  
339 more likely to occur. Relative humidity increases with decreasing altitudes, which indicates that droplets are less likely to be  
340 completely evaporated at the lower altitude. The combined effects of the three factors determine the entrainment-mixing  
341 vertical evolution.

342

343 It is noteworthy that the traditional homogeneous mixing degrees are still useful properties to quantify entrainment-mixing  
344 mechanisms, if adiabatic values of microphysical properties are properly determined. The new homogeneous mixing degree  
345 defined here provides an alternative method to quantify entrainment-mixing mechanisms by overcoming difficulties of  
346 determining adiabatic microphysical properties needed in the traditional approaches. This new method can be applied to other  
347 datasets since the new definition is based on theoretical understanding of entrainment-mixing mechanisms, which is not limited  
348 to the dataset used here. It would be interesting to apply this method to other stratocumulus and cumulus observations in  
349 different climate zones.

350



351 **Code and Data Availability**

352 The codes can be accessed by contacting Chunsong Lu via [luchunsong110@gmail.com](mailto:luchunsong110@gmail.com). The POST data is available on  
353 <https://archive.eol.ucar.edu/projects/post/>.

354

355 **Author Contributions**

356 SG performed the data analysis and manuscript writing. CL proposed the idea, guided this work and modified the  
357 manuscript. YL and SSY supervised this work and helped revise the manuscript. JZ and LZ offered helps to the data  
358 analysis. ND and YM also contributed to the modification of manuscript.

359

360 **Competing Interests**

361 The authors declare that they have no conflict of interest.

362



363 **Appendix A**

364 Turbulent dissipation rate ( $\varepsilon$ ) is calculated by three dimensional wind velocities (Meischner et al., 2001)

365 
$$\varepsilon \approx \frac{D_{NN}^{3/2}}{(4.01m)^{3/2}d},$$

366 (A1)

367 with  $m \approx 0.2(2\pi)^{2/3}$  (Panofsky, 1984).  $D_{NN}$  is the local spatial structure function using three wind components and is defined  
368 as:

369 
$$D_{NN}(t, d) = \frac{1}{3} \left\{ \frac{8}{7} \left[ u(t) - u\left(t - \frac{d}{TAS}\right) \right]^2 + \frac{8}{7} \left[ v(t) - v\left(t - \frac{d}{TAS}\right) \right]^2 + \left[ w(t) - w\left(t - \frac{d}{TAS}\right) \right]^2 \right\}, \quad (A2)$$

370 where three wind components, east, north and vertical, are represented by  $u$ ,  $v$  and  $w$ , respectively; TAS is the aircraft true air  
371 speed ( $\sim 55 \text{ m s}^{-1}$ );  $t$  is the time;  $d$  is the scale parameter:

372 
$$d = TAS \Delta t. \quad (A3)$$

373 where  $\Delta t$  is the time interval, which is set to 0.1 s.

374



375 **Appendix B**

376 The parameter  $A$  in equation (10) is

377 
$$A = \frac{1}{\left[\left(\frac{L_h}{R_v T} - 1\right) \frac{L_h \rho_L}{KT} + \frac{\rho_L R_v T}{D e_s(T)}\right]}, \quad (\text{B1})$$

378 where  $R_v$ ,  $L_h$ ,  $T$ ,  $K$ ,  $\rho_L$ ,  $D$ , and  $e_s(T)$  are water vapor specific gas constant, latent heat, temperature, coefficient of air thermal  
379 conductivity coefficient, liquid water density, water vapor diffusion coefficient in air and vapor pressure of saturation,  
380 respectively.

381



382 **Acknowledgment**

383 The authors thank the crew of the POST campaign. This research was supported by the National Natural Science Foundation  
384 of China (41822504, 42027804, 42075073, 41975181), the National Key Research and Development Program of China  
385 (2019YFA0606803) and Qinglan Project (R2018Q05).  
386



387 **References**

- 388 Andrejczuk, M., Grabowski, W. W., Malinowski, S. P., and Smolarkiewicz, P. K.: Numerical Simulation of Cloud–Clear Air  
389 Interfacial Mixing: Homogeneous versus Inhomogeneous Mixing, *Journal of the Atmospheric Sciences*, 66, 2493-2500,  
390 10.1175/2009jas2956.1, 2009.
- 391 Baker, M., and Latham, J.: The evolution of droplet spectra and the rate of production of embryonic raindrops in small cumulus  
392 clouds, *Journal of the Atmospheric Sciences*, 36, 1612-1615, 1979.
- 393 Baker, M., Corbin, R., and Latham, J.: The influence of entrainment on the evolution of cloud droplet spectra: I. A model of  
394 inhomogeneous mixing, *Quarterly Journal of the Royal Meteorological Society*, 106, 581-598, 10.1002/qj.49710644914, 1980.
- 395 Baker, M., Breidenthal, R., Choullarton, T., and Latham, J.: The effects of turbulent mixing in clouds, *Journal of the atmospheric*  
396 *sciences*, 41, 299-304, 10.1175/1520-0469(1984)041<0299:TEOTMI>2.0.CO;2, 1984.
- 397 Bony, S., and Dufresne, J. L.: Marine boundary layer clouds at the heart of tropical cloud feedback uncertainties in climate  
398 models, *Geophysical Research Letters*, 32, 10.1029/2005GL023851, 2005.
- 399 Burnet, F., and Brenguier, J.-L.: Observational study of the entrainment-mixing process in warm convective clouds, *Journal of*  
400 *the atmospheric sciences*, 64, 1995-2011, 10.1175/JAS3928.1, 2007.
- 401 Carman, J., Rossiter, D., Khelif, D., Jonsson, H., Faloon, I., and Chuang, P.: Observational constraints on entrainment and the  
402 entrainment interface layer in stratocumulus, *Atmospheric Chemistry and Physics*, 12, 11135-11152, 2012.
- 403 Cess, R. D., Potter, G., Blanchet, J., Boer, G., Ghan, S., Kiehl, J., Le Treut, H., Li, Z.-X., Liang, X.-Z., and Mitchell, J.:  
404 Interpretation of cloud-climate feedback as produced by 14 atmospheric general circulation models, *Science*, 245, 513-516,  
405 10.1126/science.245.4917.513, 1989.
- 406 Deng, Z., Zhao, C., Zhang, Q., Huang, M., and Ma, X.: Statistical analysis of microphysical properties and the parameterization  
407 of effective radius of warm clouds in Beijing area, *Atmospheric Research*, 93, 888-896, 2009.
- 408 Freud, E., Rosenfeld, D., Andreae, M., Costa, A., and Artaxo, P.: Robust relations between CCN and the vertical evolution of  
409 cloud drop size distribution in deep convective clouds, *Atmospheric Chemistry and Physics*, 8, 1661-1675, 2008.
- 410 Freud, E., Rosenfeld, D., and Kulkarni, J. R.: Resolving both entrainment-mixing and number of activated CCN in deep  
411 convective clouds, *Atmospheric Chemistry and Physics*, 11, 12887-12900, 10.5194/acp-11-12887-2011, 2011.
- 412 Gao, W., Sui, C. H., Fan, J., Hu, Z., and Zhong, L.: A study of cloud microphysics and precipitation over the Tibetan Plateau  
413 by radar observations and cloud - resolving model simulations, *Journal of Geophysical Research Atmospheres*, 121, 13,735-  
414 713,752, 2016.
- 415 Gao, Z., Liu, Y., Li, X., and Lu, C.: Investigation of turbulent entrainment - mixing processes with a new particle - resolved  
416 direct numerical simulation model, *Journal of Geophysical Research: Atmospheres*, 123, 2194-2214, 2018.
- 417 Gerber, H., Frick, G., Malinowski, S. P., Kumala, W., and Krueger, S.: POST—A new look at stratocumulus, *American*  
418 *Meteorological Society 13th Conference on Cloud Physics*, 2010.
- 419 Gerber, H., Frick, G., Malinowski, S. P., Jonsson, H., Khelif, D., and Krueger, S. K.: Entrainment rates and microphysics in  
420 POST stratocumulus, *Journal of Geophysical Research: Atmospheres*, 118, 12,094-012,109, 2013.
- 421 Gerber, H., Malinowski, S. P., and Jonsson, H.: Evaporative and radiative cooling in POST stratocumulus, *Journal of the*  
422 *Atmospheric Sciences*, 73, 3877-3884, 2016.
- 423 Gerber, H. E., Frick, G. M., Jensen, J. B., and Hudson, J. G.: Entrainment, mixing, and microphysics in trade-wind cumulus,  
424 *Journal of the Meteorological Society of Japan. Ser. II*, 86, 87-106, 10.2151/jmsj.86A.87, 2008.
- 425 Grabowski, W. W.: Indirect impact of atmospheric aerosols in idealized simulations of convective–radiative quasi equilibrium,  
426 *Journal of climate*, 19, 4664-4682, 10.1175/JCLI3857.1, 2006.
- 427 Haman, K. E., Malinowski, S. P., Kurowski, M. J., Gerber, H., and Brenguier, J.-L.: Small scale mixing processes at the top of  
428 a marine stratocumulus—a case study, *Quarterly Journal of the Royal Meteorological Society*, 133, 213-226, 10.1002/qj.5,  
429 2007.
- 430 Hill, S. A., Krueger, S., Gerber, H., and Malinowski, S.: Entrainment interface layer of stratocumulus-topped boundary layers  
431 during POST, 13 AMS Conf. On Cloud Phys, 2010.
- 432 Hoffmann, F., and Feingold, G.: Entrainment and Mixing in Stratocumulus: Effects of a New Explicit Subgrid-Scale Scheme  
433 for Large-Eddy Simulations with Particle-Based Microphysics, *Journal of the Atmospheric Sciences*, 76, 1955-1973,



- 434 10.1175/jas-d-18-0318.1, 2019.
- 435 Hudson, James, G., Yum, Seong, and Soo: Droplet spectral broadening in marine stratus, *Journal of the Atmospheric Sciences*,  
436 1997.
- 437 Jarecka, D., Grabowski, W. W., Morrison, H., and Pawlowska, H.: Homogeneity of the subgrid-scale turbulent mixing in large-  
438 eddy simulation of shallow convection, *Journal of the atmospheric sciences*, 70, 2751-2767, 2013.
- 439 Jen-La Plante, I., Ma, Y., Nurowska, K., Gerber, H., Khelif, D., Karpinska, K., Kopec, M. K., Kumala, W., and Malinowski,  
440 S. P.: Physics of Stratocumulus Top (POST): turbulence characteristics, *Atmospheric Chemistry and Physics*, 16, 9711, 2016.
- 441 Jensen, J., Austin, P., Baker, M., and Blyth, A.: Turbulent mixing, spectral evolution and dynamics in a warm cumulus cloud,  
442 *Journal of the atmospheric sciences*, 42, 173-192, 10.1175/1520-0469(1985)042<0173:TMSEAD>2.0.CO;2, 1985.
- 443 Kumala, W., Haman, K., Kopec, M., Khelif, D., and Malinowski, S.: Modified ultrafast thermometer UFT-M and temperature  
444 measurements during Physics of Stratocumulus Top (POST), *Atmospheric Measurement Techniques*, 6, 2043-2054, 2013.
- 445 Kumar, B., Janetzko, F., Schumacher, J. R., and Shaw, R. A.: Extreme responses of a coupled scalar-particle system during  
446 turbulent mixing, *New Journal of Physics*, 14, 115020, 2012.
- 447 Kumar, B., Schumacher, J., and Shaw, R. A.: Cloud microphysical effects of turbulent mixing and entrainment, *Theoretical  
448 and Computational Fluid Dynamics*, 27, 361-376, 10.1007/s00162-012-0272-z, 2013.
- 449 Kumar, B., Götzfried, P., Suresh, N., Schumacher, J., and Shaw, R. A.: Scale Dependence of Cloud Microphysical Response  
450 to Turbulent Entrainment and Mixing, *Journal of Advances in Modeling Earth Systems*, 10, 2777-2785, 2018.
- 451 Lasher - trapp, S. G., Cooper, W. A., and Blyth, A. M.: Broadening of droplet size distributions from entrainment and mixing  
452 in a cumulus cloud, *Quarterly Journal of the Royal Meteorological Society: A journal of the atmospheric sciences, applied  
453 meteorology and physical oceanography*, 131, 195-220, 10.1256/qj.03.199, 2005.
- 454 Lehmann, K., Siebert, H., and Shaw, R. A.: Homogeneous and Inhomogeneous Mixing in Cumulus Clouds: Dependence on  
455 Local Turbulence Structure, *Journal of the Atmospheric Sciences*, 66, 3641-3659, 10.1175/2009jas3012.1, 2009.
- 456 Liu, Y., Daum, P. H., Chai, S. K., and Liu, F.: Cloud parameterizations, cloud physics, and their connections: an overview,  
457 Brookhaven National Lab., Upton, NY (US), 2002.
- 458 Lu, C., Liu, Y., and Niu, S.: Examination of turbulent entrainment - mixing mechanisms using a combined approach, *Journal  
459 of Geophysical Research: Atmospheres*, 116, 10.1029/2011JD015944, 2011.
- 460 Lu, C., Liu, Y., Niu, S., and Vogelmann, A. M.: Lateral entrainment rate in shallow cumuli: Dependence on dry air sources and  
461 probability density functions, *Geophysical Research Letters*, 39, 2012.
- 462 Lu, C., Liu, Y., and Niu, S.: A method for distinguishing and linking turbulent entrainment mixing and collision-coalescence  
463 in stratocumulus clouds, *Chin. Sci. Bull.*, 58, 545-551, 2013a.
- 464 Lu, C., Liu, Y., Niu, S., Krueger, S., and Wagner, T.: Exploring parameterization for turbulent entrainment-mixing processes  
465 in clouds, *Journal of Geophysical Research Atmospheres*, 118, 185-194, 2013b.
- 466 Lu, C., Niu, S., Liu, Y., and Vogelmann, A. M.: Empirical relationship between entrainment rate and microphysics in cumulus  
467 clouds, *Geophysical Research Letters*, 40, 2333-2338, 10.1002/grl.50445, 2013c.
- 468 Lu, C., Liu, Y., and Niu, S.: Entrainment-mixing parameterization in shallow cumuli and effects of secondary mixing events,  
469 *Science China Press*, 2014a.
- 470 Lu, C., Liu, Y., Niu, S., and Endo, S.: Scale dependence of entrainment-mixing mechanisms in cumulus clouds, *Journal of  
471 Geophysical Research: Atmospheres*, 119, 13,877-813,890, 10.1002/2014jd022265, 2014b.
- 472 Lu, C., Liu, Y., Zhu, B., Yum, S. S., Krueger, S. K., Qiu, Y., Niu, S., and Luo, S.: On Which Microphysical Time Scales to Use  
473 in Studies of Entrainment - Mixing Mechanisms in Clouds, *Journal of Geophysical Research: Atmospheres*, 123, 3740-3756,  
474 2018.
- 475 Ma, Y.-F., Malinowski, S. P., Karpinska, K., Gerber, H. E., and Kumala, W.: Scaling analysis of temperature and liquid water  
476 content in the marine boundary layer clouds during POST, *Journal of the Atmospheric Sciences*, 74, 4075-4092, 2017.
- 477 Ma, Y. F., Pedersen, J., Grabowski, W., Kopec, M., and Malinowski, S.: Influences of Subsidence and Free - Tropospheric  
478 Conditions on the Nocturnal Growth of Nonclassical Marine Stratocumulus, *Journal of Advances in Modeling Earth Systems*,  
479 10, 2706-2730, 2018.
- 480 Malinowski, S. P., Haman, K., Kumala, W., Kopec, M., Gerber, H., and Krueger, S.: Smallscale variability of temperature and



- 481 LWC at stratocumulus top, 13 AMS Conf. On Cloud Phys., th, 2010.
- 482 Malinowski, S. P., Gerber, H., Jen-La Plante, I., Kopec, M. K., Kumala, W., Nurowska, K., Chuang, P. Y., Khelif, D., and  
483 Haman, K. E.: Physics of Stratocumulus Top (POST): turbulent mixing across capping inversion, *Atmospheric Chemistry and*  
484 *Physics*, 13, 12171-12186, 2013.
- 485 Meischner, P., Baumann, R., and Holler, H.: Eddy Dissipation Rates in Thunderstorms Estimated by Doppler Radar in Relation  
486 to Aircraft In Situ Measurements, *Journal of Atmospheric & Oceanic Technology*, 18, 1609-1627, 2001.
- 487 Morrison, A. G.: Advanced Two-Moment Bulk Microphysics for Global Models. Part I: Off-Line Tests and Comparison with  
488 Other Schemes, *Journal of Climate*, 28, 1288-1307, 2015.
- 489 Panofsky, H. A.: *Atmospheric turbulence, Models and methods for engineering applications.*, 397, 1984.
- 490 Pawlowska, H., Brenguier, J., and Burnet, F.: Microphysical properties of stratocumulus clouds, *Atmospheric research*, 55, 15-  
491 33, 10.1016/S0169-8095(00)00054-5, 2000.
- 492 Siebert, H., Franke, H., Lehmann, K., Maser, R., Saw, E. W., Schell, D., Shaw, R. A., and Wendisch, M.: Probing finescale  
493 dynamics and microphysics of clouds with helicopter-borne measurements, *Bull. Amer. Meteor. Soc.*, 87, 1727-1738, 2006.
- 494 Small, J. D., Chuang, P. Y., and Jonsson, H. H.: Microphysical imprint of entrainment in warm cumulus, *Tellus B: Chemical*  
495 *and Physical Meteorology*, 65, 19922, 2013.
- 496 Stephens, G. L.: Cloud feedbacks in the climate system: A critical review, *Journal of climate*, 18, 237-273, 10.1175/JCLI-  
497 3243.1, 2005.
- 498 Su, C.-W., Krueger, S. K., McMurtry, P. A., and Austin, P. H.: Linear eddy modeling of droplet spectral evolution during  
499 entrainment and mixing in cumulus clouds, *Atmospheric research*, 47, 41-58, 10.1016/S0169-8095(98)00039-8, 1998.
- 500 Telford, J.: Clouds with turbulence; the role of entrainment, *Atmospheric research*, 40, 261-282, 10.1016/0169-  
501 8095(95)00038-0, 1996.
- 502 Telford, J. W., and Chai, S. K.: A new aspect of condensation theory, *pure and applied geophysics*, 118, 720-742,  
503 10.1007/bf01593025, 1980.
- 504 Wang, J., Daum, P. H., Yum, S. S., Liu, Y., Senum, G. I., Lu, M.-L., Seinfeld, J. H., and Jonsson, H.: Observations of marine  
505 stratocumulus microphysics and implications for processes controlling droplet spectra: Results from the Marine  
506 Stratus/Stratocumulus Experiment, *Journal of Geophysical Research*, 114, 10.1029/2008jd011035, 2009.
- 507 Wang, Y.: *Aerosol-Cloud Interactions from Urban, Regional, to Global Scales*, Springer, 2015.
- 508 Wang, Y., Niu, S., Lv, J., Lu, C., Xu, X., Wang, Y., Ding, J., Zhang, H., Wang, T., and Kang, B.: A new method for distinguishing  
509 unactivated particles in cloud condensation nuclei (CCN) measurements: Implications for aerosol indirect effect evaluation,  
510 *Geophysical Research Letters*, 2019.
- 511 Wood, R.: Stratocumulus clouds, *Monthly Weather Review*, 140, 2373-2423, 2012.
- 512 Wyngaard, J. C.: *Turbulence in the Atmosphere*, Cambridge University Press, 2010.
- 513 Xu, X., and Xue, H.: Impacts of free-tropospheric temperature and humidity on nocturnal nonprecipitating marine  
514 stratocumulus, *Journal of the Atmospheric Sciences*, 72, 2853-2864, 2015.
- 515 Xu, X., Lu, C., Liu, Y., Gao, W., Wang, Y., Cheng, Y., Luo, S., and Weverberg, K. V.: Effects of Cloud Liquid - Phase  
516 Microphysical Processes in Mixed - Phase Cumuli Over the Tibetan Plateau, *Journal of Geophysical Research: Atmospheres*,  
517 125, 2020.
- 518 Xue, H., and Feingold, G.: Large-eddy simulations of trade wind cumuli: Investigation of aerosol indirect effects, *Journal of*  
519 *the Atmospheric Sciences*, 63, 1605-1622, 10.1175/JAS3706.1, 2006.
- 520 Yau, M. K., and Rogers, R. R.: *A short course in cloud physics*, Elsevier, 1996.
- 521 Yeom, J. M., Yum, S. S., Liu, Y., and Lu, C.: A study on the entrainment and mixing process in the continental stratocumulus  
522 clouds measured during the RACORO campaign, *Atmospheric Research*, 194, 89-99, 10.1016/j.atmosres.2017.04.028, 2017.
- 523 Yum, S. S., Wang, J., Liu, Y., Senum, G., Springston, S., McGraw, R., and Yeom, J. M.: Cloud microphysical relationships and  
524 their implication on entrainment and mixing mechanism for the stratocumulus clouds measured during the VOCALS project,  
525 *Journal of Geophysical Research: Atmospheres*, 120, 5047-5069, 10.1002/2014jd022802, 2015.
- 526 Zhang, Q., Quan, J., Tie, X., Huang, M., and Ma, X.: Impact of aerosol particles on cloud formation: Aircraft measurements  
527 in China, *Atmos. Environ.*, 45, 665-672, 2011.



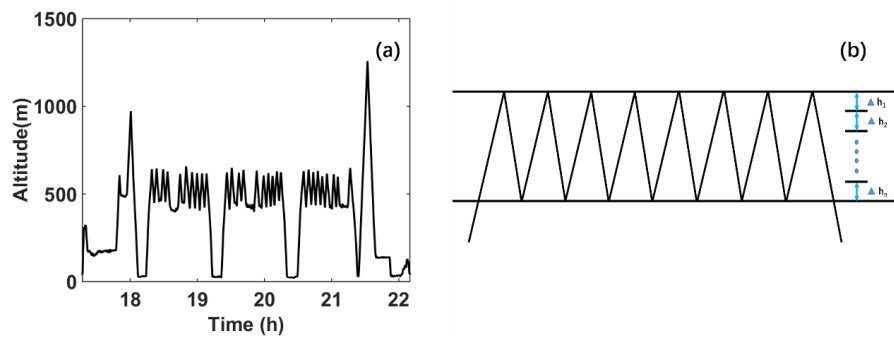
- 528 Zhao, C., and Garrett, T. J.: Effects of Arctic haze on surface cloud radiative forcing, *Geophysical Research Letters*, 42, 557-  
529 564, 2015.
- 530 Zheng, Y., and Rosenfeld, D.: Linear relation between convective cloud base height and updrafts and application to satellite  
531 retrievals, *Geophysical Research Letters*, 42, 6485-6491, 2015.  
532



533 **Table 1.** List of different methods determining adiabatic values

Number	Methods
1	<p>LWC<sub>a</sub>: calculated from the adiabatic growth from cloud base;</p> <p>n<sub>a</sub>: maximum number concentration in each level;</p> <p>r<sub>va</sub>: calculated by <math>r_{va} = \sqrt[3]{\frac{LWC_a}{\frac{4}{3}\pi\rho_L n_a}}</math>.</p>
2	<p>LWC<sub>a</sub>: calculated from the adiabatic growth from cloud base;</p> <p>r<sub>va</sub>: maximum volume mean radius in each level;</p> <p>n<sub>a</sub>: calculated by <math>n_a = \frac{LWC_a}{\frac{4}{3}\pi\rho r_{va}^3}</math>.</p>
3	<p>LWC<sub>a</sub>: maximum liquid water content in each level</p> <p>n<sub>a</sub>: maximum number concentration in each level;</p> <p>r<sub>va</sub>: calculated by <math>r_{va} = \sqrt[3]{\frac{LWC_a}{\frac{4}{3}\pi\rho n_a}}</math>.</p>
4	<p>LWC<sub>a</sub>: maximum liquid water content in each level;</p> <p>r<sub>va</sub>: maximum volume mean radius in each level;</p> <p>n<sub>a</sub>: calculated by <math>n_a = \frac{LWC_a}{\frac{4}{3}\pi\rho r_{va}^3}</math>.</p>
5	<p>n<sub>a</sub>: maximum number concentration in the interval;</p> <p>r<sub>va</sub>: maximum volume mean radius in the interval;</p> <p>LWC<sub>a</sub>: calculated by <math>LWC_a = \frac{4}{3}\pi\rho r_{va}^3 n_a</math>.</p>

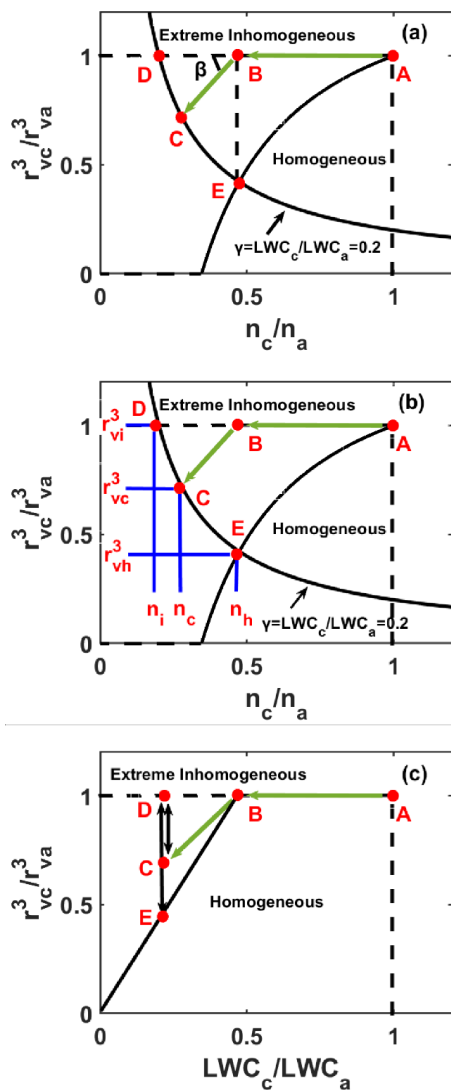
534



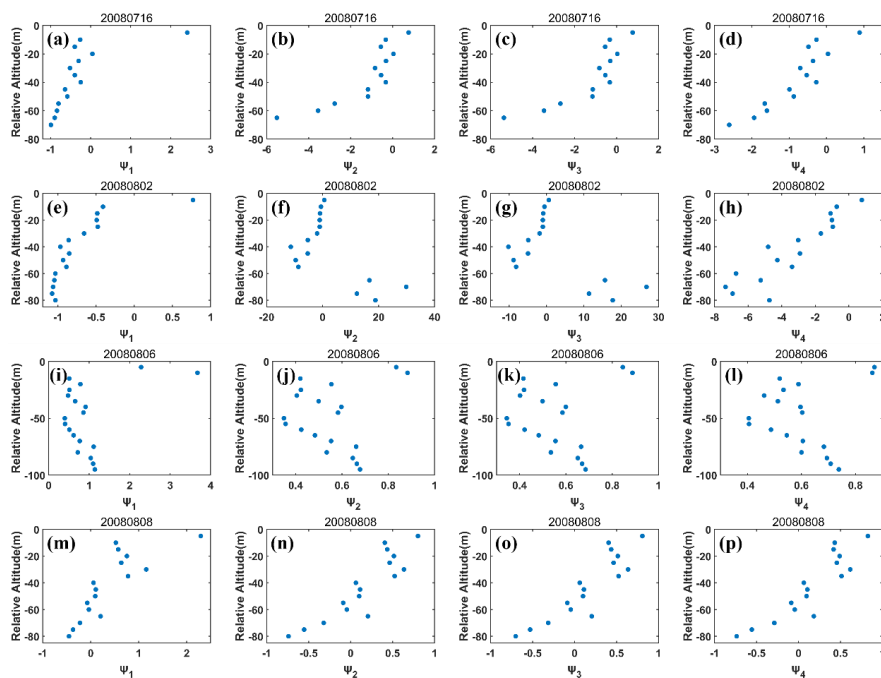
535

536 **Figure 1.** (a) Flight track on 16 July 2008. (b) Altitude stratification procedure of the sawtooth patterns, with the mean vertical resolution of

537 5 m such that  $\Delta h_1 = \Delta h_2 = \dots = \Delta h_n = 5$  m.

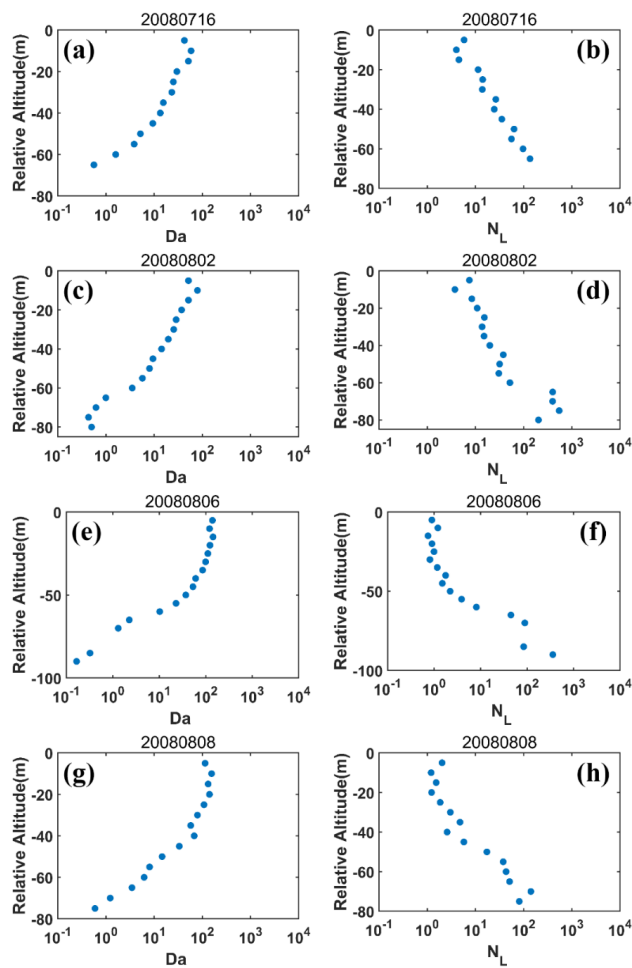


538  
 539 **Figure 2.** Microphysical diagram interpreting the definition for different homogeneous mixing degrees ((a)  $\psi_1$ ; (b)  $\psi_2, \psi_3$ ; (c)  $\psi_4$ ). The  
 540 Points A and B represent the adiabatic state and the state after entrainment, respectively. If the extreme inhomogeneous mixing process  
 541 occurs, the cloud state approaches Point D; if the homogeneous mixing process occurs, the cloud state approaches Point E. The actual mixing  
 542 and evaporation processes are between the two extremes and cloud state approaches Point C. Extreme inhomogeneous mixing process is  
 543 represented by the horizontal dashed line; homogeneous mixing process is represented by the solid line starting from Point A in (a) and (b),  
 544 and the solid line starting from Point B in (c). Another black line in (a) and (b) corresponds to contour of  $\gamma = 0.2$  defined as the ratio of liquid  
 545 water content ( $LWC_c$ ) to its adiabatic value ( $LWC_a$ ). The vertical dashed line represents the x-axis property equal to 1. The horizontal blue  
 546 solid lines represent the y-axis properties of Point D ( $r_{vi}^3$ ), Point C ( $r_{vc}^3$ ) and Point E ( $r_{vh}^3$ ). The vertical blue solid lines represent the x-axis  
 547 properties of Point D ( $n_i$ ), Point C ( $n_c$ ) and Point E ( $n_h$ ). See text for the meanings of other symbols.



548

549 **Figure 3.** Height dependence of the first homogeneous mixing degree ( $\psi_1$ ) on (a) 16 July 2008, (e) 02 August 2008, (i) 06 August 2008 and  
550 (m) 08 August 2008; height dependence of the second homogeneous mixing degree ( $\psi_2$ ) on (b) 16 July 2008, (f) 02 August 2008, (j) 06  
551 August 2008 and (n) 08 August 2008; height dependence of the third homogeneous mixing degree ( $\psi_3$ ) on (c) 16 July 2008, (g) 02 August  
552 2008, (k) 06 August 2008 and (o) 08 August 2008; and the fourth homogeneous mixing degree ( $\psi_4$ ) on (d) 16 July 2008, (h) 02 August  
553 2008, (l) 06 August 2008 and (p) 08 August 2008. The relative altitude on the y-axis equal to 0 represents the cloud tops. Adiabatic liquid water  
554 content ( $LWC_a$ ) is obtained by the adiabatic growth from cloud base, adiabatic number concentration ( $n_a$ ) is assumed to be the maximum  
555 volume mean radius at each level, and adiabatic volume mean radius ( $r_{va}$ ) is calculated with  $LWC_a$  and  $r_{va}$ .



556

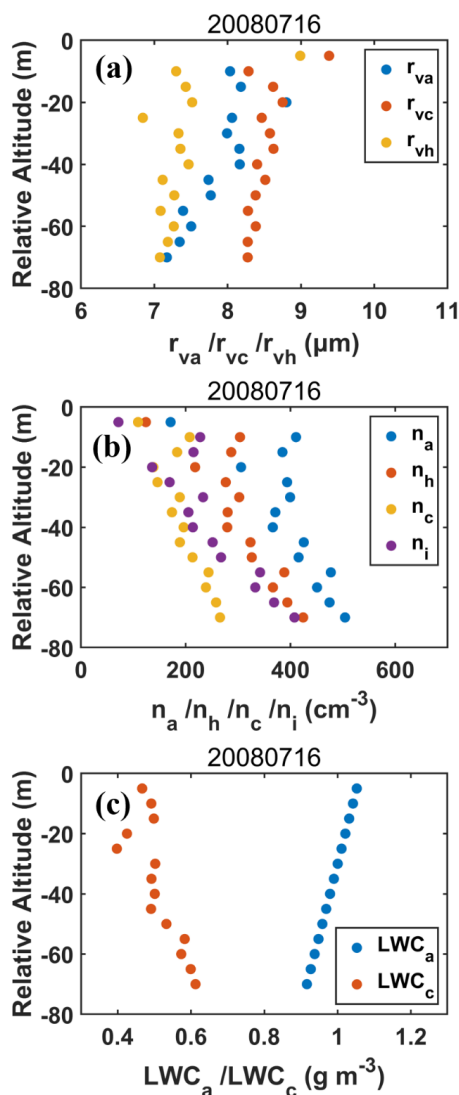
557 **Figure 4.** Height dependence of Damkohler number ( $Da$ ) on (a) 16 July 2008, (c) 02 August 2008, (e) 06 August 2008 and (g) 08 August

558 2008; height dependence of transition scale number ( $N_L$ ) on (b) 16 July 2008, (d) 02 August 2008, (f) 06 August 2008 and (h) 08 August

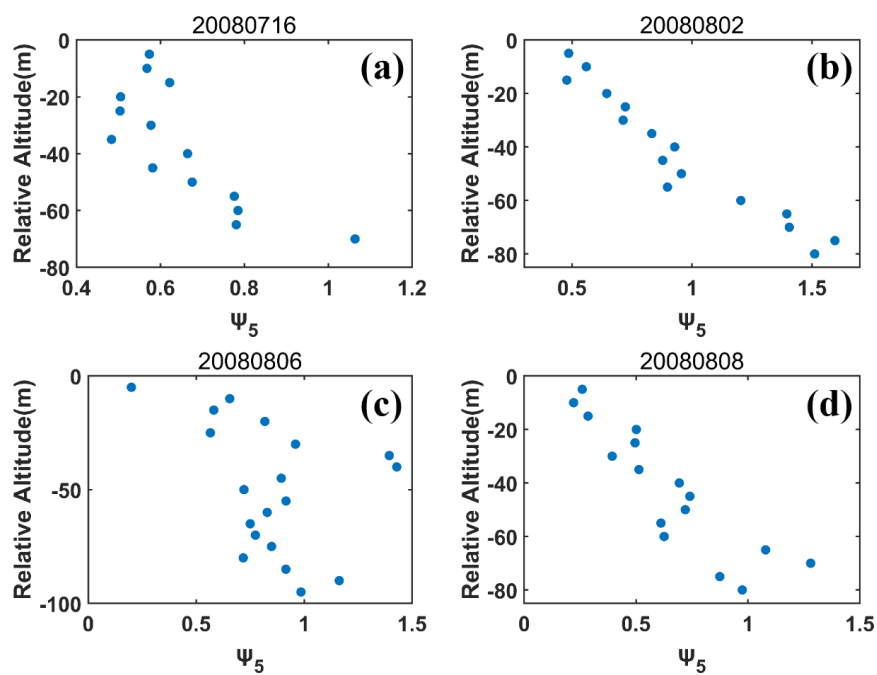
559 2008. The relative altitude on the y-axis equal to 0 represents the cloud tops. Adiabatic liquid water content ( $LWC_a$ ) is obtained by the

560 adiabatic growth from cloud base, adiabatic number concentration ( $n_a$ ) is assumed to be the maximum volume mean radius at each level,

561 and adiabatic volume mean radius ( $r_{va}$ ) is calculated with  $LWC_a$  and  $r_{va}$ .



562  
 563 **Figure 5.** Height dependence of (a)  $r_{va}$ ,  $r_{vc}$ ,  $r_{vh}$ , (b)  $n_a$ ,  $n_h$ ,  $n_c$ ,  $n_i$  and (c)  $\text{LWC}_a$ ,  $\text{LWC}_c$  on 16 July 2008. The relative altitude on the y-axis  
 564 equal to 0 represents the cloud tops. Adiabatic liquid water content ( $\text{LWC}_a$ ) is obtained by the adiabatic growth from cloud base, the maximum  
 565 number concentration at each level is assumed to be adiabatic number concentration ( $n_a$ ), and adiabatic volume radius ( $r_{va}$ ) is calculated with  
 566  $\text{LWC}_a$  and  $n_a$ .

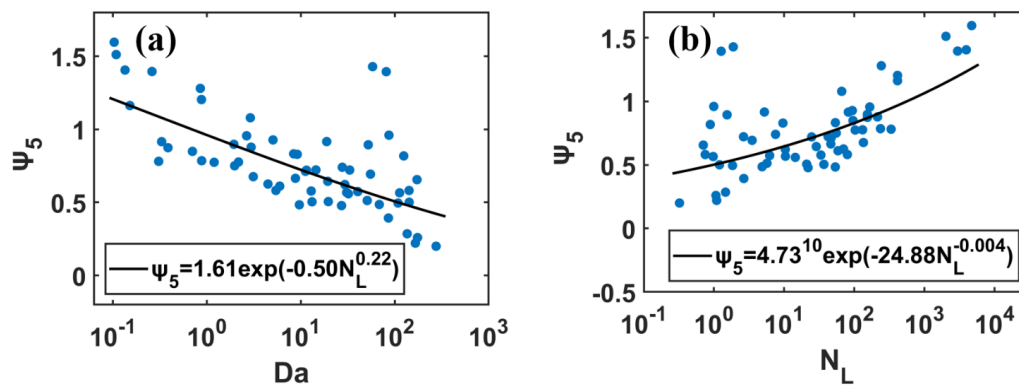


567

568 **Figure 6.** Height dependence of the newly defined homogeneous mixing degree ( $\psi_5$ ) on (a) 16 July 2008, (b) 02 August 2008, (c) 06 August

569 2008 and (d) 08 August 2008. The relative altitude on the y-axis equal to 0 represents the cloud tops.

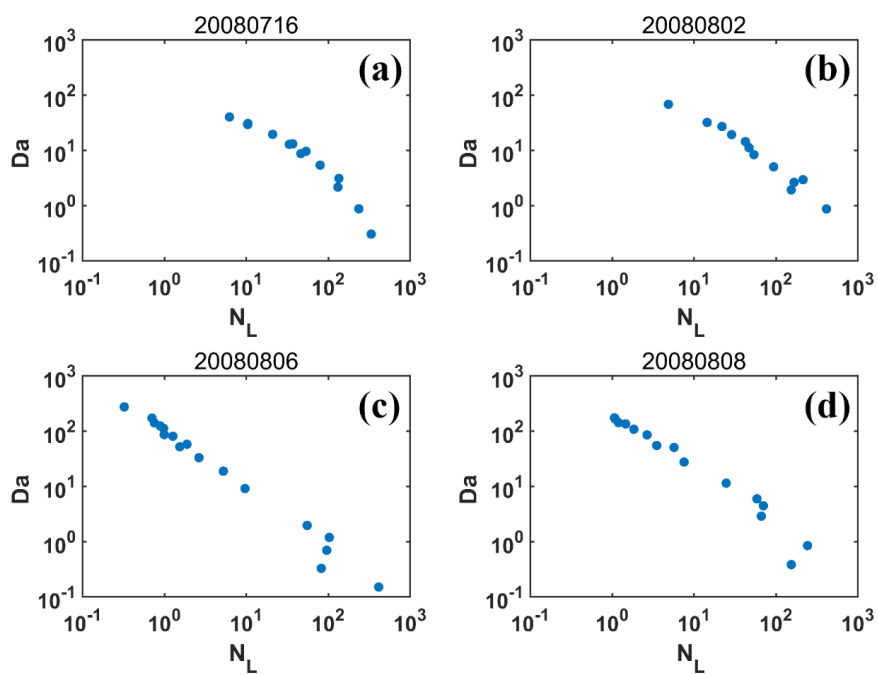
570



571

572 **Figure 7.** Relationships of the newly defined homogeneous mixing degree ( $\psi_5$ ) versus (a) Damkohler number ( $Da$ ) and (b) transition scale

573 number ( $N_L$ ).

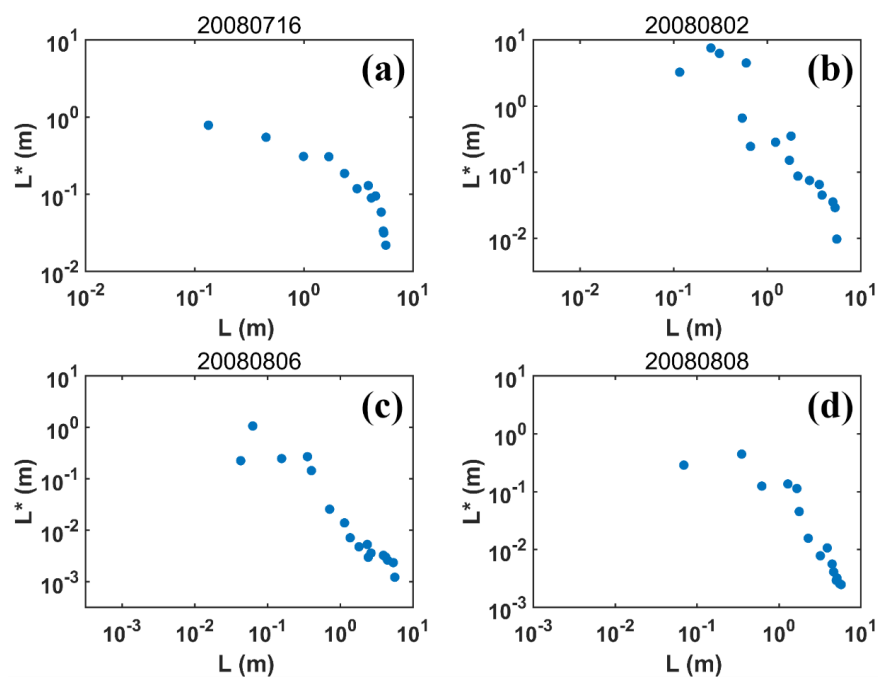


574

575 **Figure 8.** Relationships of Damkohler number ( $Da$ ) versus transition scale number ( $N_L$ ) on (a) 16 July 2008, (b) 02 August 2008, (c) 06

576 August 2008 and (d) 08 August 2008.

577

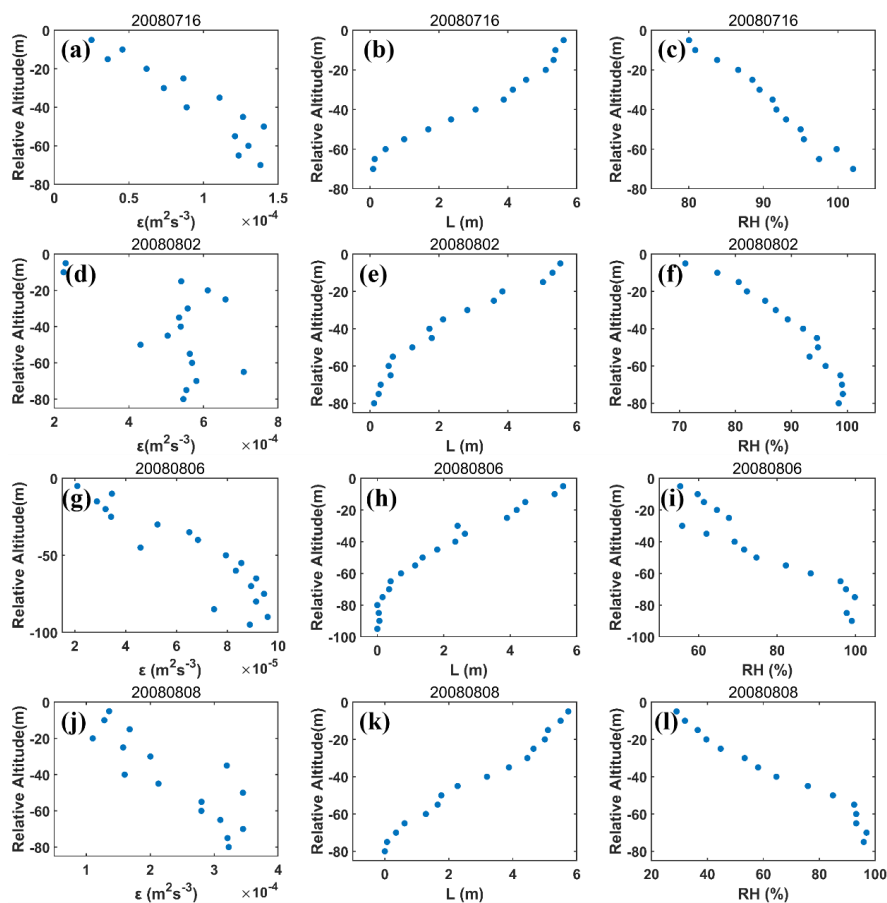


578

579 **Figure 9.** Relationships of transitional scale ( $L^*$ ) versus droplet-free air length ( $L$ ) on (a) 16 July 2008, (b) 02 August 2008, (c) 06 August

580 2008 and (d) 08 August 2008.

581



582

583 **Figure 10.** Height dependence of dissipation rate ( $\epsilon$ ) on (a) 16 July 2008, (d) 02 August 2008, (g) 06 August 2008 and (j) 08 August 2008;

584 height dependence of relative humidity (RH) of droplet-free air on (b) 16 July 2008, (e) 02 August 2008, (h) 06 August 2008 and (k) 08

585 August 2008; and height dependence of length of droplet-free air ( $L$ ) on (c) 16 July 2008, (f) 02 August 2008, (i) 06 August 2008 and (l) 08

586 August 2008. The relative altitude on the y-axis equal to 0 represents the cloud tops.

587